Acta Crystallographica Section A
Foundations of Crystallography
ISSN 0108-7673

Received 27 October 2011
Accepted 13 January 2012

Higher-dimensional crystallography of *N*-fold quasiperiodic tilings

Sofia Deloudi* and Walter Steurer

Laboratory of Crystallography, Department of Materials, ETH Zurich, Wolfgang-Pauli-Strasse 10, 8093 Zurich, Switzerland. Correspondence e-mail: deloudi@mat.ethz.ch

Crystallography and periodic average structures (PASs) of two-dimensional (2D) quasiperiodic tilings with *N*-fold symmetry (*N*-QPTs with N = 7, 8, 9, 10, 11, 12, 13, 15) were studied using the higher-dimensional approach. By identifying the best (most representative) PASs for each case, it was found that the complexity of the PASs and the degree of average periodicity (DAP) strongly depend on the dimensionality and topology of the hypersurfaces (HSs) carrying the structural information. The distribution of deviations from periodicity is given by the HSs projected upon physical space. The 8-, 10- and 12-QPTs with their 2D HSs have the highest DAP. In the case of the 7-, 9-, 11-, 13- and 15-QPTs, the dimensionality of the HSs is greater than two, and is therefore reduced in the projection upon 2D physical space. This results in a non-homogeneous distribution of deviations from the periodic average lattice, and therefore in a higher complexity of the PASs. Contrary to the 7- and 9-QPTs, which still have representative PASs and DAPs, the 11-, 13- and 15-QPTs have a very low DAP.

1. Introduction

The discovery of quasicrystals induced a paradigm change in crystallography. Quasicrystals with decagonal or icosahedral diffraction symmetry and sharp Bragg reflections questioned one of the fundamentals of diffraction theory: the assumption that three-dimensional lattice periodicity was a necessary condition for pure point Fourier spectra. It was shown that *d*D quasiperiodic structures, which can be described as *d*D sections of *n*D periodic hypercrystal structures ($d < n$), also have pure point Fourier spectra; for an introduction to the field see, for instance, Steurer & Deloudi (2008) and Steurer & Deloudi (2009). On tiling theory, model sets and diffraction properties see, for instance, de Bruijn (1981), Moody & Patera (2000) and Baake & Grimm (2011).

Owing to the lack of a point of global *N*-fold symmetry in general quasiperiodic tilings (QPTs), their symmetry is usually given in terms of their diffraction symmetry, *i.e.* the point symmetry of their diffraction pattern (Laue group) or of the Patterson function. In our case of two-dimensional (2D) *N*-QPTs, the diffraction symmetry as well as the orientational symmetry of the tiling edges is *N*-fold if N is an even number and 2*N*-fold if N is an odd number.

The study of quasiperiodic structures and their underlying tilings is not only of crystallographic interest. The possibility to design quasiperiodic structures with arbitrarily high rotational symmetries *and* Bragg diffraction spectra opens up new opportunities for the creation of metacrystals such as photonic and phononic heterostructures, with omnidirectional bandgaps. For a review see, for instance, Steurer & Sutter-Widmer (2007). However, the implications of quasiperiodicity on the physical properties of a system have not all been fully explored yet.

Why are quasicrystals with specific diffraction symmetries such as decagonal or icosahedral stable and those with octagonal or dodecagonal symmetry less favorable or even metastable only? Why has no other rotational symmetry ever been observed in an intermetallic quasicrystal? Is there a correlation between the stability of quasicrystals and the embedding dimension of their structures? How does the order of the rotational symmetry N or the kind of the number N (prime *versus* non-prime, for example) play into this? The study of periodic average structures (PASs) of QPTs allows contributions to these fundamental questions from a geometrical point of view. Specifically, it provides a tool for the classification of QPTs according to their degree of average periodicity (DAP).

A PAS results from a proper projection of a QPT within the higher-dimensional approach. It can be described by a periodic average lattice (PAL) decorated with projected hypersurfaces (PHSs) so that all vertices of the respective QPT lie within the boundaries of the PHSs. A close periodic approximation of a QPT by one of the infinitely many possible PASs is given if the PHSs are small (small deviation of the tiling vertices from the PAL nodes) and if at the same time the average occupancy factor of the PAS ($p_{\rm PAS}$) is close to 1.

Steurer & Haibach (1999) demonstrated the existence of discrete PASs for the three prototypes of quasicrystal structures: the 1D Fibonacci sequence, the 2D Penrose tiling and the 3D Ammann tiling. By providing lattices closely related to the respective QPTs, PASs are of particular importance, for

instance, for the understanding of quasicrystal-to-crystal phase transformations (Steurer, 2000) and quasicrystal–crystal interfaces (Weisskopf *et al.*, 2007).

The oblique-projection method proposed for the derivation of PASs by Steurer & Haibach (1999) allows the investigation of QPTs of any symmetry and dimensionality. Later, it was applied to QPTs with eight-, ten-, 12- and 14-fold diffraction symmetry as well (Sutter-Widmer *et al.*, 2007*a*,*b*). It was shown that PASs allow the prediction of band gaps in phononic quasicrystals depending on their DAP.

With the discovery of a self-assembled colloidal water-based mesoscopic quasicrystal with 18-fold diffraction symmetry (Fischer *et al.*, 2011), the investigation of PASs was extended to the ninefold QPT. Phase transitions between this phase, another quasiperiodic phase with 12-fold diffraction symmetry, and a face-centered-cubic (f.c.c.) phase, were observed for this system. The close correlation between the two quasicrystalline phases and the f.c.c phase could be visualized *via* their closely related PASs.

In order to identify a general trend of the DAP of QPTs regarding dimensionality and rotational symmetry, we extended the study of PASs to 11-, 13- and 15-fold QPTs. In addition, we give in the following a detailed representation and discussion of the PASs of the aforementioned axial QPTs (Sutter-Widmer *et al.*, 2007*a*,*b*; Fischer *et al.*, 2011).

There are several fully equivalent ways to generate QPTs within the higher-dimensional approach: the strip-projection method and the embedding method. We use the former for the derivation of the window, which defines the hypersurfaces (HSs) in the latter. Furthermore, in both methods either a reducible (canonical) or an irreducible basis can be employed. In the following, we will use an irreducible basis for the eight- and tenfold QPTs, and a reducible basis for all other QPTs. Of course, the resulting PASs do not depend on the approach used. The derivation method for PASs will be described in §2.

QPTs and their PASs will be discussed in groups according to their higher-dimensional description. The 8- and 10-QPTs are given in §4. They are the simplest cases, each one having only a single 2D HS and the minimal dimension 4 (this is also the rank of the vector module spanned by the reciprocal-space basis).

In §5, the second group is treated, 7-, 11- and 13- QPTs of rank 6, 10 and 12, respectively. The HSs for each of these tilings are given by equidistant cuts of the window. The HSs have the dimensions 4, 8 and 10, and are highly symmetric, simple, convex polytopes.

The third and last group (§6) examines the 12-, 9- and 15-QPTs of rank 4, 6 and 8, respectively. Like in the group before, the HSs are given by equidistant cuts of the window perpendicular to the redundant dimensions in the canonical description. Unlike the cases in the second group, there is not only one redundant dimension (the diagonal of the window) but additional directions to which the HSs are perpendicular, resulting in HSs with maximal dimension 2, 4 and 6. The complex distribution of HSs in higher-dimensional space is visualized with multidimensional combined scaling plots (MCS plots, see §3).

The formulae needed for an analytic calculation of the structure factors of the infinite systems are given by Steurer & Deloudi (2009) for HSs of dimensions 2, 3 and 4. For HSs of higher dimensions, they can be derived employing the same method. These cumbersome derivations can be avoided by calculating the Fourier coefficients of patches of QPTs, with their size adjusted to the needed accuracy.

2. Derivation of PASs

The nD embedding space $\mathbf{V} = \mathbf{V}^{\parallel} \oplus \mathbf{V}^{\perp}$ consists of two orthogonal subspaces, the 2D physical space $\mathbf{V}^{\parallel}$, also called par(allel)-space, and the $(n-2)$D internal space $\mathbf{V}^{\perp}$, also called perp(endicular)-space. In this Cartesian nD embedding space spanned by the $\mathbf{V}$ basis, we define the basis of a hyperlattice ($\mathbf{D}$ basis) given by vectors $\mathbf{d}_i$ ($i = 1, \ldots, n$). The nD reciprocal basis $\mathbf{D}^*$ is given by vectors $\mathbf{d}_i^*$ ($i = 1, \ldots, n$), and is related to the direct basis by the condition $\mathbf{d}_i \cdot \mathbf{d}_j^* = \delta_{ij}$. Orthogonal projection of $\mathbf{D}^*$ onto physical space gives an n-star of 2D reciprocal basis vectors $\mathbf{a}_i^*$ ($i = 1, \ldots, n$), spanning a Z-module of rank n. The nD diffraction vectors are defined as $\mathbf{H} = (\mathbf{H}^{\parallel}, \mathbf{H}^{\perp}) = \sum_{i=1}^{n} h_i \mathbf{d}_i^*$ and $\mathbf{H}^{\parallel} = \sum_{i=1}^{n} h_i \mathbf{a}_i^*$.

The derivation of a PAS works the same way for the nD embedding method with an irreducible and with a canonical basis. In both cases, orthogonal projection of the direct or reciprocal hyperlattice onto dD par-space gives a dense set of points. This is different in the case of an oblique projection along rational directions, where all vertices of an nD hyperlattice project onto the nodes of a dD sublattice, the PAL of the QPT (Steurer & Haibach, 1999). The HSs that decorate the hyperlattice in the nD embedding method are projected upon par-space in the same way as the lattice vertices, resulting in a discrete set of PHSs. The deviation of the tiling vertices from the PAL nodes is always within the boundaries of the PHSs.

The projection onto dD direct space corresponds to a dD section of the reciprocal hyperlattice in Fourier space, containing a sublattice of diffraction vectors. The ratio of the sum of Bragg reflection intensities $\mathbf{I}_{\mathrm{PAS}}$ of the cut space to the total sum of reflection intensities $\mathbf{I}_{\mathrm{QPT}}$ is a measure of the representativeness of the PAS.

The PAS for a given QPT with $d = 2$ can be derived in the following way:

(*a*) Choose two strong Bragg reflections with linearly independent diffraction vectors $\mathbf{H}_1^{\parallel}$ and $\mathbf{H}_2^{\parallel}$. They span a sublattice of diffraction vectors representing the Fourier transform of the PAS. In nD, the corresponding reciprocal-space vectors, $\mathbf{H}_1$ and $\mathbf{H}_2$, span the 2D cut space of the nD reciprocal space.

(*b*) Find $(n-2)$ linearly independent vectors, $\mathbf{P}_j^*$, perpendicular to the cut space, with $\mathbf{P}_j^* = \sum_{i=1}^{n} p_{ji} \mathbf{d}_i^*$, $j = 1, \ldots, (n-2)$. Then the vectors $\mathbf{P}_j = \sum_{i=1}^{n} p_{ji} \mathbf{d}_i$ give the $(n-2)$ projection directions. The projection onto $\mathbf{V}^{\parallel}$ is performed along $\mathbf{P}_j$.

The point-group symmetry of the PAS, which is always a crystallographic one, is necessarily lower than that of dD QPTs with non-crystallographic symmetries. Consequently, a one-to-one mapping of the tiling vertices to the lattice nodes

of the PAL is impossible for topological reasons. Some of the PAL nodes are not related to any tiling vertex, and some are related to more than one. The QPT can therefore be described as a displacive and occupational (density) modulation of its underlying PAL.

Since the point densities of a QPT and its PAS have to be equal, we can define $p_{\rm PAS}$ as the ratio between the point density of the QPT and that of the PAL. The point density of a QPT can be calculated as the ratio of the volume of the HSs and the volume of the nD unit cell of the hyperlattice.

In general, a QPT has infinitely many PASs (Cervellino & Steurer, 2002). The geometrically best, *i.e.* most representative, PAS will have a lattice parameter $a_{\rm PAS}$ comparable with the edge length of the unit tiles a_r, and $p_{\rm PAS}$ close to 1. The size of the PHSs is a measure of the deviation of the QPT from its PAL. The smaller the PHSs are and the closer $p_{\rm PAS}$ is to 1, the higher is the DAP of the QPT.

Once the unit-cell parameters of the PAS of a quasiperiodic structure are known, the PAS can as well be obtained by taking the QPT vertices modulo this unit cell. All vertices are mapped into the PHSs. But, while a PAS is unambiguously defined by the cut space that is spanned by the two chosen diffraction vectors in higher dimensions, this is not the case for a PAS that is generated remaining in par-space only. In higher dimensions, each choice of two diffraction vectors among the complete set of diffraction vectors that lie in one cut space will result in identical PASs. Generating a PAS while remaining only in par-space, however, will result in the same size and shape of PHSs, but different edge lengths of the average lattice and therefore different $p_{\rm PAS}$. It is therefore important to always choose the smallest possible basis in reciprocal par-space for a certain cut space.

3. Multidimensional combined scaling (MCS) plot

The MCS plot is a way of visualizing the topology and distribution of HSs in the nD hypercubic lattice for QPTs of high dimensionality and complexity. The HSs for all tilings in §6 are depicted in MCS plots.

The perp-space is divided into 2D subspaces, each given by pairs of basis vectors of the $\mathbf{V}$ basis. We distinguish between subspaces, in which the HSs have a volume, and the redundant dimensions, in which the HSs occupy specific positions and have zero volume. If there is more than one subspace, in which the HSs project into geometrically equivalent shapes (identical image except for a permutation of the vertices), only one of those subspaces will be visualized.

Orthogonal projection of the HSs on any non-redundant subspace gives overlapping HSs centered around zero. Combining this plot with an orthogonal projection upon a redundant subspace means centering each projection of the HSs around its position in the redundant subspace. Adequate scaling of the two subspaces makes sure that there are no overlaps of HSs belonging to different positions in the visualization. In the case of further redundant dimensions, however, there will be still HSs which are centered around the same position and overlap. Then, the next redundant subspace can be combined into the plot, which splits up those HSs in return. Again, adequate scaling is used. This procedure can be repeated for any number of dimensions, until every HS is centered around its distinct position, and there are no overlaps. Finally, a plot is obtained which is 2D in total, but visualizes the topology of the HSs in nD.

4. Octagonal and decagonal tilings (8- and 10-QPTs)

4.1. Formalism

Both the 8- [often referred to as the Ammann–Beenker tiling; see Ammann *et al.* (1992)] and the 10-QPT have 4D minimum embedding spaces. Each one consists of two 2D orthogonal subspaces $\mathbf{V}^{\parallel}$ and $\mathbf{V}^{\perp}$. The 2D par-space reciprocal basis vectors are given by $\mathbf{a}_i^* = a^*[\cos(2\pi i/8), \sin(2\pi i/8)]$, with $i = 1, \ldots, 4$. The 4D hyperlattice of the 8-QPT is spanned by the basis vectors

$$\mathbf{d}_i = \frac{1}{2a^*}\begin{pmatrix} \cos\frac{2\pi i}{8} \\ \sin\frac{2\pi i}{8} \\ \cos\frac{6\pi i}{8} \\ \sin\frac{6\pi i}{8} \end{pmatrix}_{\mathbf{V}}, \quad \text{with } i = 1, \ldots, 4. \tag{1}$$

The HS of the 8-QPT is an octagon defined by the vectors $\mathbf{a}_i^{\rm HS}$, with

$$\mathbf{a}_i^{\rm HS} = \frac{1}{2a^*}\left(1 + \frac{1}{2^{1/2}}\right)^{1/2}\begin{pmatrix} 0 \\ 0 \\ \cos\frac{(2i-1)\pi}{8} \\ \sin\frac{(2i-1)\pi}{8} \end{pmatrix}_{\mathbf{V}}, \quad \text{with } i = 1, \ldots, 8. \tag{2}$$

The unit tiles edge length a_r is related to the length a^* of the 2D par-space reciprocal basis vectors by $a_r = 1/2a^*$, and the lattice spanned by the vectors $\mathbf{d}_i$ is hypercubic.

An example of an 8-QPT and its generating HS is depicted in Fig. 1,[1] with vertices colored according to their coordination. The partition of the HS, *i.e.* the subdivision in parts that generate vertices with the same coordination, is indicated by the color code of the tiling. The diffraction pattern is shown in Fig. 2.

The basis of the 4D hyperlattice of the 10-QPT is defined as

$$\mathbf{d}_i = \frac{2}{5a^*}\begin{pmatrix} \cos\frac{2i\pi}{5} - 1 \\ \sin\frac{2i\pi}{5} \\ \cos\frac{6i\pi}{5} - 1 \\ \sin\frac{6i\pi}{5} \end{pmatrix}_{\mathbf{V}}, \quad \text{with } i = 1, \ldots, 4, \tag{3}$$

and the 2D par-space reciprocal basis vectors are given by $\mathbf{a}_i^* = a^*[\cos(2\pi i/10), \sin(2\pi i/10)]$, with $i = 1, \ldots, 4$. The HS of the 10-QPT is a decagon given by the vectors $\mathbf{a}_i^{\rm HS}$, with

$$\mathbf{a}_i^{\rm HS} = \frac{2}{5a^*}\,\gamma\,\frac{(5+5^{1/2})^{1/2}}{2^{1/2}}\begin{pmatrix} 0 \\ 0 \\ \cos\left(\frac{i\pi}{5} + \frac{\pi}{2}\right) \\ \sin\left(\frac{i\pi}{5} + \frac{\pi}{2}\right) \end{pmatrix}_{\mathbf{V}}, \tag{4}$$

[1] Larger versions of all of the figures presented in this paper have been deposited in the IUCr electronic archives (Reference: DM5021). Services for accessing these data are described at the back of the journal.

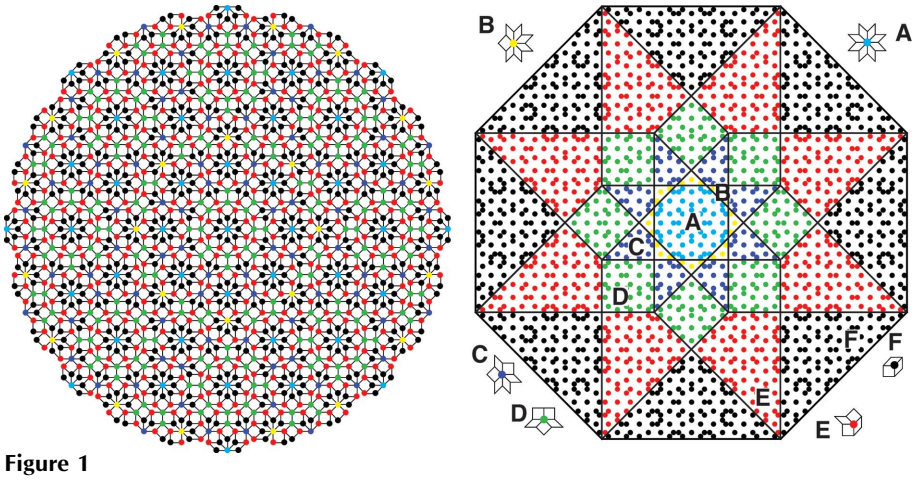

Figure 1
(Left) 8-QPT with the six different vertex types color-coded. This 8-QPT, with squares and rhombs as unit tiles, corresponds to that described by Socolar (1989). (Right) Partitioning of the HS located at the origin of the 4D hypercubic unit cell shown together with the six vertex configurations A–F. Each point of the HS corresponds to one vertex of the tiling.

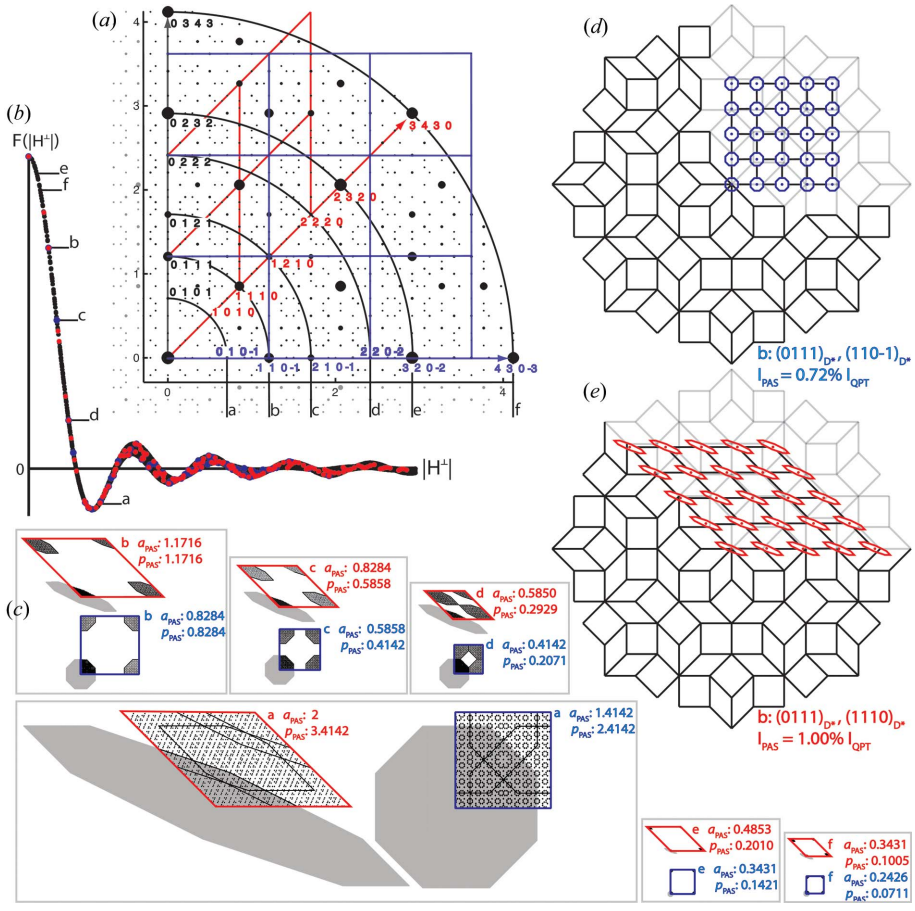

Figure 2
(*a*) Diffraction pattern of the 8-QPT in par-space. The diffraction vectors of the investigated PASs are located on circles marked by letters a–f. The reciprocal lattices for two different combinations of diffraction vectors of type b are shown in red and blue, respectively. Diffraction vectors on these grids lie on the corresponding cut planes in *n*D reciprocal space. (*b*) Structure factors $F(|\mathbf{H}^{\perp}|)$ of 8-QPT as a function of $|\mathbf{H}^{\perp}|$. There is only one branch of $F(|\mathbf{H}^{\perp}|)$, as expected for a single HS positioned on the origin of the hypercrystal structure. (*c*) Vertices of the 8-QPT modulo one unit cell of different PAS denoted with blue and red indices in (*a*), and PHS. Lattice parameters, *l* in units of a_r, and $p_{\rm PAS}$ are given in the figure. (*d*, *e*): 8-QPT with overlaid PAS defined by the diffraction vectors $(0111)_{\mathbf{D}^*}$; $(110\bar{1})_{\mathbf{D}^*}$ (*d*) and $(0111)_{\mathbf{D}^*}$; $(1110)_{\mathbf{D}^*}$ (*e*) shown in blue/red in (*a*). The small blue/red undistorted/distorted octagons on the grids correspond to PHS. $\mathbf{I}_{\rm PAS}$ is given relative to $\mathbf{I}_{\rm QPT}$.

where i runs from 1 to 10 and $1 < \gamma < \tau$. Different classes of 10-QPTs can be generated for different values of γ, and therewith for different resulting sizes of the HS (see Masakova *et al.*, 2005). Values outside this range give τ-scaled tilings, but no new tiling classes. As an example, a tiling generated with γ = 1.117 is depicted in Fig. 3. It is the DT_1/VT_1 tiling according to Masakova *et al.* (2005), containing copies of five different kinds of Delone tiles: a small and a large pentagon, two different isosceles triangles and a trapezoid. The Delone tiles have two different edge lengths corresponding to the edge lengths of the small and large pentagon. a_r is defined as the edge length of the large pentagon, with $a_r = 2/5a^*$. The lattice spanned by the vectors $\mathbf{d}_i$ is hyperrhombohedral; it would be hypercubic in the 5D reducible description.

4.2. PASs

In Fig. 2, the structure factors of the 8-QPT are shown as a function of $|\mathbf{H}^{\perp}|$ and $|\mathbf{H}^{\parallel}|$. Letters a–f in Fig. 2(*a*) mark symmetrically equivalent reflections (chosen for the derivation of the different PASs), which lie on circles with radius $|\mathbf{H}^{\parallel}|$. Symmetrically equivalent reflections all have the same value of $|\mathbf{H}^{\perp}|$. In the following, we describe two non-equivalent variants of choosing the PAS-defining pairs of diffraction vectors. One leads to a rhombic unit cell of the PAS, the other to a square one. The indices of the diffraction vectors defining each PAS are listed in Fig. 2.

The best PASs for the 8-QPT are defined by reflections with strong intensities on the circle marked by the letter b in Fig. 2(*a*). The PHSs and the tiling modulo one unit cell (dotted part of the HS) are given in Fig. 2(*c*) for each PAS. The relationships between the two best PASs and the respective tilings are illustrated in Figs. 2(*d*) and 2(*e*). The sum of intensities in the cut space is approximately 0.7 and 1%, respectively, of the total intensity for these two PASs. Each type of PAS represents therefore approximately 3% and 4%, respectively, of the total diffraction intensity, if the four equivalent orientations of the PAS

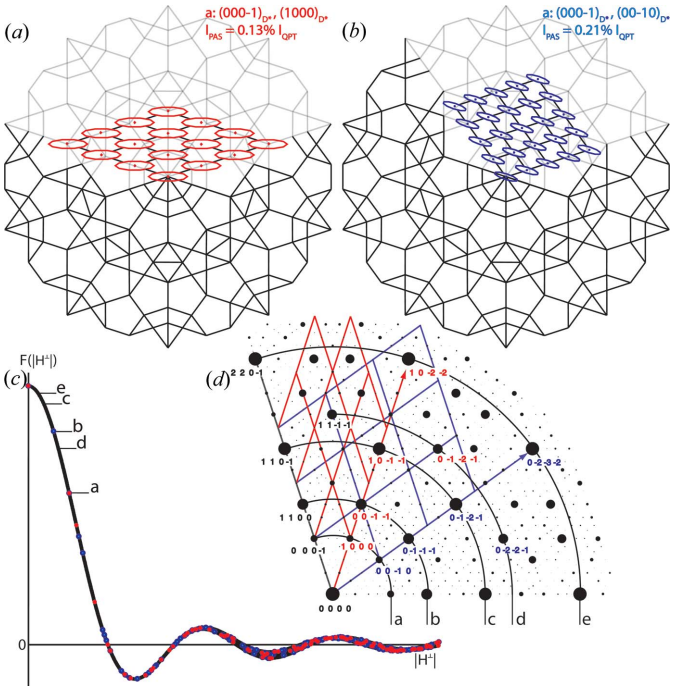

Figure 3
The 10-QPTs shown in (*a*) and (*b*) consist of copies of five different kinds of Delone tiles: a small and a large pentagon, two isosceles triangles and a trapezoid. $a_r = 1$ refers to the edge length of the large pentagon. The tilings are overlaid with the two best PASs. The decagonal HS have been distorted by the oblique projection. $p_{\rm PAS}$ is 1.4727 for the PAS depicted in red, and 0.9102 for the PAS in blue. $\mathbf{I}_{\rm PAS}$ is given relative to $\mathbf{I}_{\rm QPT}$. (*c*) Structure factors of the 10-QPT as a function of $|\mathbf{H}^{\perp}|$. There is only one branch of $F(|\mathbf{H}^{\perp}|)$ as expected for a single HS positioned on the origin of the hypercrystal structure. (*d*) Diffraction pattern of the 10-QPT in par-space. The diffraction vectors of the investigated PASs are located on circles marked by letters a–e. The reciprocal lattices for two different combinations of diffraction vectors of type a are shown in red and blue, respectively. Diffraction vectors on these grids lie on the corresponding cut planes in *n*D reciprocal space. Note that the diffraction vector $(00\bar{1}\bar{1})_{\mathbf{D}^*}$, marked with the letter b, also lies on the cut space defined by the blue grid.

are taken into account. The PAS marked by the letter d in Fig. 2(*a*) has the same cut space as the PAS marked by the letter b. It visualizes the importance of choosing the smallest possible diffraction vectors as basis of the cut space, if one generates the PAS by a modulo function, as discussed at the end of §2. Here, the wrong choice of basis vectors generates a PAS with too small edge length.

In the case of the 10-QPT, among all possible PASs resulting from reflections with strong intensities that have been investigated, the best one is based on the pair of diffraction vectors $(000\bar{1})_{\mathbf{D}^*}$ and $(00\bar{1}0)_{\mathbf{D}^*}$. In this PAS [blue grid in Fig. 3(*d*), blue PHSs in Fig. 3(*b*)], only 9% of all PAL nodes do not correspond to tiling vertices. The PAS resulting from the symmetrically equivalent reflections defining the red grid in Fig. 3(*d*) and the red PHSs in Fig. 3(*b*) has a much larger $p_{\rm PAS}$ of 1.4727 as well as larger PHSs, that means larger deviations of the tiling vertices from the PAL nodes. Both tilings discussed in this section have a high DAP.

5. Heptagonal, hendecagonal and triskaidecagonal tilings (7-, 11- and 13-QPTs)

5.1. Formalism

All diffraction vectors $\mathbf{H}^{\parallel}$ of *N*-QPTs, with $N = 7$, 11 and 13, can be represented on a 2D basis with vectors $\mathbf{a}_i^* = a^*[\cos(2\pi i/N), \sin(2\pi i/N)]$, with $i = 1, \ldots, N$. The projected *n*D diffraction vectors are given by $\mathbf{H}^{\parallel} = \sum_{i=1}^{N} h_i \mathbf{a}_i^*$. Based on the number of independent reciprocal basis vectors necessary to index the reflections with integers, the rank of the *Z*-module and the dimension of the embedding spaces in their irreducible variants results to 6, 10 or 12, respectively. For the 6D irreducible representation of the sevenfold tiling, see Steurer & Deloudi (2009). We will use the reducible canonical setting in the following.

The 7D hypercubic lattice (**D** basis) of the 7-QPT is defined by the vectors

$$\mathbf{d}_i = \frac{2}{7a^*}\begin{pmatrix} \cos(2\pi i/7) \\ \sin(2\pi i/7) \\ \cos(4\pi i/7) \\ \sin(4\pi i/7) \\ \cos(6\pi i/7) \\ \sin(6\pi i/7) \\ 1/\sqrt{2} \end{pmatrix}_{\mathbf{V}}, \quad \text{with } i = 1, \ldots, 7. \tag{5}$$

The unit tiles edge length a_r is related to the length a^* of the 2D par-space reciprocal basis vectors by $a_r = 2/7a^*$. The vectors $\mathbf{v}_0$ and $\mathbf{w}_0$ span the 2D par-space $\mathbf{V}^{\parallel}$, $\mathbf{v}_k$ and $\mathbf{w}_k$ span $\mathbf{V}_k^{\perp}$ with $k = 1, 2$, and $\mathbf{d}$ spans $\mathbf{V}_3^{\perp}$, with $\mathbf{V} = \mathbf{V}^{\parallel} \oplus \mathbf{V}^{\perp} = \mathbf{V}^{\parallel} \oplus \mathbf{V}_1^{\perp} \oplus \mathbf{V}_2^{\perp} \oplus \mathbf{V}_3^{\perp}$. In the **D** basis, they can be expressed as $\mathbf{v}_k = (2/7)^{1/2}(1/a^*)\cos[(k+1)2\pi i/7]_{\mathbf{D}}$, $\mathbf{w}_k = (2/7)^{1/2}(1/a^*)\sin[(k+1)2\pi i/7]_{\mathbf{D}}$, with $k = 1, \ldots, 2$, and $\mathbf{d} = [1/(7a^*)^{1/2}](1111111)_{\mathbf{D}}$.

The 11- and 13-QPTs show a similar division in subspaces as the 7-QPT, with the extension of $\mathbf{V}^{\perp}$ by two and three 2D subspaces, respectively.

11-QPT: $\mathbf{v}_k$ and $\mathbf{w}_k$ span $\mathbf{V}_k^{\perp}$ for $k = 1, \ldots, 4$, and $\mathbf{d}$ spans $\mathbf{V}_5^{\perp}$. $\mathbf{V}$ is given by $\mathbf{V} = \mathbf{V}^{\parallel} \oplus \mathbf{V}^{\perp} = \mathbf{V}^{\parallel} \oplus \mathbf{V}_1^{\perp} \oplus \mathbf{V}_2^{\perp} \oplus \mathbf{V}_3^{\perp} \oplus \mathbf{V}_4^{\perp} \oplus \mathbf{V}_5^{\perp}$. It is $\mathbf{v}_k = (2/11)^{1/2}(1/a^*)\cos[(k+1)2\pi i/11]_{\mathbf{D}}$, $\mathbf{w}_k = (2/11)^{1/2}(1/a^*)\sin[(k+1)2\pi i/11]_{\mathbf{D}}$ and $\mathbf{d} = (1/11^{1/2}a^*) \times (11111111111)_{\mathbf{D}}$.

The *n*D hypercubic lattice (**D** basis) is given by the vectors

$$\mathbf{d}_i = \frac{2}{11a^*}\begin{pmatrix} \cos(2\pi i/11) \\ \sin(2\pi i/11) \\ \cos(4\pi i/11) \\ \sin(4\pi i/11) \\ \cos(6\pi i/11) \\ \sin(6\pi i/11) \\ \cos(8\pi i/11) \\ \sin(8\pi i/11) \\ \cos(10\pi i/11) \\ \sin(10\pi i/11) \\ 1/\sqrt{2} \end{pmatrix}_{\mathbf{V}}, \quad \text{with } i = 1, \ldots, 11. \tag{6}$$

The unit tiles edge length a_r is related to the length a^* of the 2D par-space reciprocal basis vectors by $a_r = 2/11a^*$.

13-QPT: $\mathbf{v}_k$ and $\mathbf{w}_k$ span $\mathbf{V}_k^{\perp}$ for $k = 1, \ldots, 5$, and $\mathbf{d}$ spans $\mathbf{V}_6^{\perp}$. $\mathbf{V}$ is then $\mathbf{V} = \mathbf{V}^{\parallel} \oplus \mathbf{V}^{\perp} = \mathbf{V}^{\parallel} \oplus \mathbf{V}_1^{\perp} \oplus \mathbf{V}_2^{\perp} \oplus \mathbf{V}_3^{\perp} \oplus \mathbf{V}_4^{\perp} \oplus \mathbf{V}_5^{\perp} \oplus \mathbf{V}_6^{\perp}$. It is $\mathbf{v}_k = (2/13)^{1/2}(1/a^*)\cos[(k+1)2\pi i/13]_{\mathbf{D}}$, $\mathbf{w}_k = (2/13)^{1/2}(1/a^*)\sin[(k+1)2\pi i/13]_{\mathbf{D}}$ and $\mathbf{d} = (1/13^{1/2}a^*) \times (1111111111111)_{\mathbf{D}}$.

The nD hypercubic lattice (**D** basis) is given by the vectors

$$\mathbf{d}_i = \frac{2}{13a^*}\begin{pmatrix} \cos(2\pi i/13) \\ \sin(2\pi i/13) \\ \cos(4\pi i/13) \\ \sin(4\pi i/13) \\ \cos(6\pi i/13) \\ \sin(6\pi i/13) \\ \cos(8\pi i/13) \\ \sin(8\pi i/13) \\ \cos(10\pi i/13) \\ \sin(10\pi i/13) \\ \cos(11\pi i/13) \\ \sin(11\pi i/13) \\ 1/\sqrt{2} \end{pmatrix}_{\mathbf{v}}, \quad \text{with } i = 1, \ldots, 13. \qquad (7)$$

The unit tiles edge length a_r is related to the length a^* of the 2D par-space reciprocal basis vectors by $a_r = 2/13a^*$.

The $(n-2)$D windows of these N-QPTs, obtained by projection of the nD unit cell onto $\mathbf{V}^{\perp}$, are zonohedra with N-fold axial symmetry (see Fig. 4). The nD strip needed in the strip-projection method is defined as an infinite extension of the window along the par-space. If a hyperlattice point is inside the strip, it generates a vertex of the tiling after projection onto $\mathbf{V}^{\parallel}$. If all hyperlattice points inside the strip are projected onto $\mathbf{V}^{\perp}$, they form n equidistant $(n-3)$D hyperplanes (polytopes) perpendicular to $\mathbf{d} = (111\ldots1)_{\mathbf{D}}$ (see Fig. 4).

These polytopes correspond to the HSs that decorate the hyperlattice in the nD embedding method. Shifts of the window along $\mathbf{d}$ result in different positions for the hyperplanes in the window and therewith in a different shape of the HSs. Three examples of such tilings are shown in Fig. 5 for the 7-QPT.

If the window is placed with its origin on the origin of the hyperlattice, the convex hull of the ith HS can be easily derived analytically. It is defined by the perp-space coordinates of the unit-cell vertices fulfilling $\sum_{j=1}^{n} a_{jk} = i$, with $i = 0, \ldots, n-1$, for the n HSs and $(a_{1k}, \ldots, a_{nk})_{\mathbf{D}}$ the kth vertex of the unit cell given in the **D** basis.

The n HSs are located at $(i/n)\mathbf{d}$, $i = 0, \ldots, n-1$, on the diagonal of the hyperrhombohedral window. The 0D HS is located at the origin ($i = 0$). Neighboring HSs are in anti-position to each other, as can be seen in Fig. 4. The $(n-1)$ HSs within the zonohedron are related by an inversion center at one half of the body diagonal. There are therefore $(N-1)/2$ independent non-zero HSs for the N-QPT, with $N =$ 7, 11 or 13, respectively.

As will be shown in §6 for the N-QPTs with $N = 9, 12$ and 15, it is possible to have several redundant dimensions, which means that the HSs are perpendicular to more than one direction in $\mathbf{V}^{\perp}$. In the same way as the HSs result as equidistant cuts perpendicular to $\mathbf{d}$, each HS is again divided into a subset of HSs perpendicular to the other redundant dimensions. This leads to a lower dimensionality of the HSs, but also to a more complex topology of their subdivided volumes.

Sevenfold symmetry is the lowest symmetry that is associated with a cubic irrational number, and shows therefore

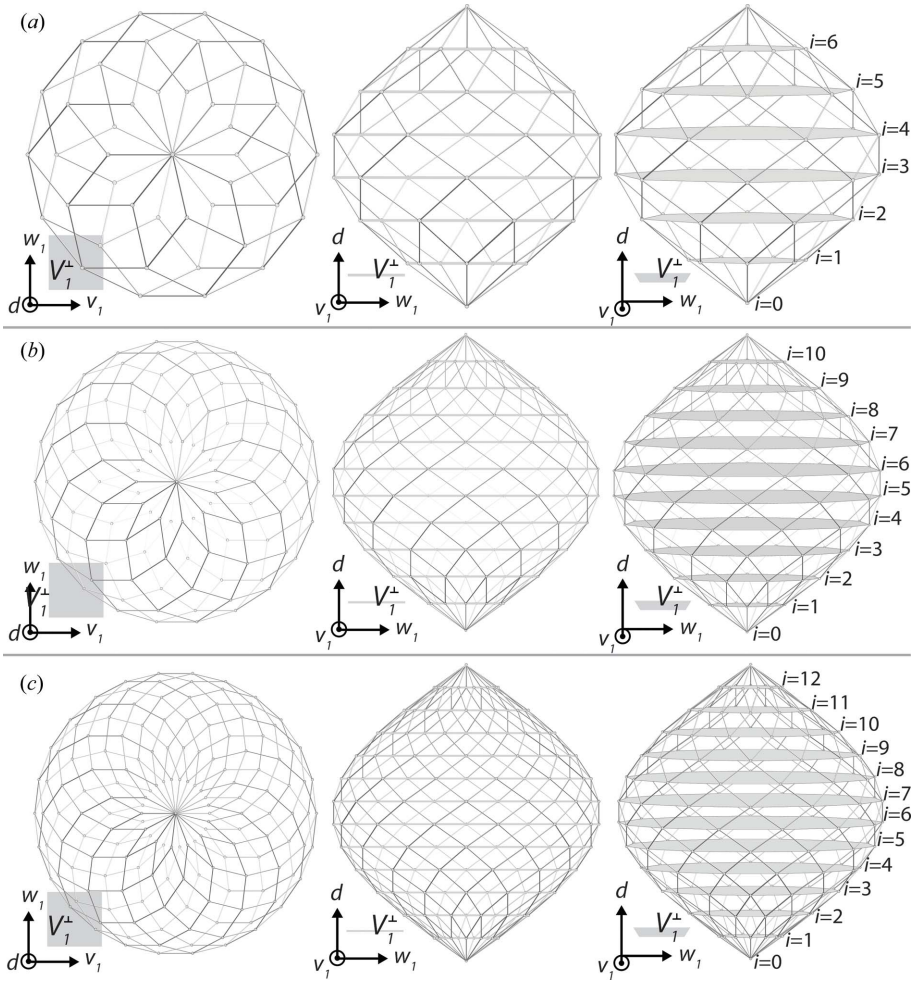

Figure 4
Projection windows of the 7-, 11- and 13-QPTs. The window of a QPT (orthogonal projection of the hyperlattice unit cell onto $\mathbf{V}^{\perp}$) is a zonohedron of dimension $n-2$. For the 7-QPT (*a*), 11-QPT (*b*) and 13-QPT (*c*), the convex hulls of the windows in the subspace spanned by $\mathbf{v}_1$, $\mathbf{w}_1$ and $\mathbf{d}$ ($\mathbf{V}_1^{\perp} \oplus \mathbf{d}$) are given in three different views: (left and middle) view along, and perpendicular to $\mathbf{d}$; (right) slightly rotated view perpendicular to $\mathbf{d}$, where the shape of the HSs is emphasized. The HSs result from n equidistant cuts of the window perpendicular to $\mathbf{d}$, at $i/7(1111111)_{\mathbf{D}}$, $i/11(11111111111)_{\mathbf{D}}$ and $i/13(1111111111111)_{\mathbf{D}}$, respectively.

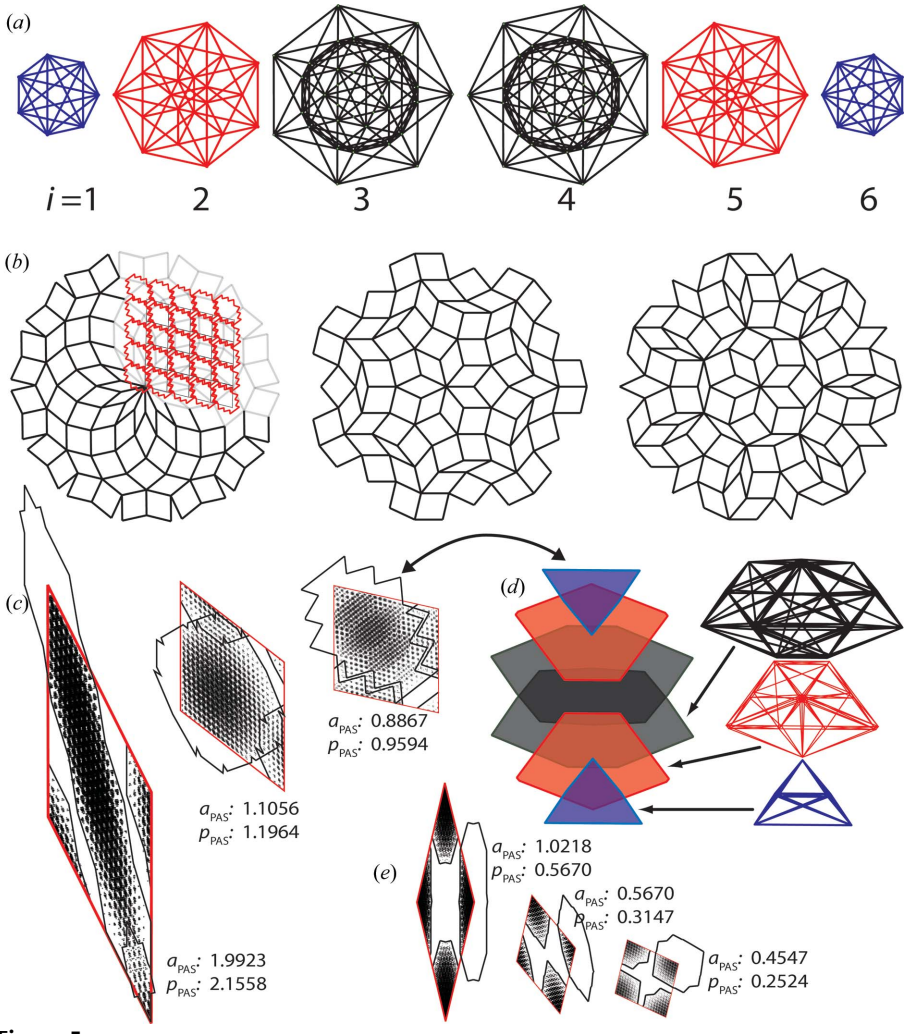

Figure 5
(*a*) The six HSs of the 7-QPT with a non-zero volume located at $i/7(1111111)_{\mathbf{D}}$, $i = 1, \ldots, 6$, in the canonical description. They are related by an inversion center in the origin and at $1/2(1111111)_{\mathbf{D}}$. The HSs are 4D polytopes shown in an orthogonal projection upon one of the two invariant subspaces of $\mathbf{V}^{\perp}$. Projection upon the second subspace results in the same image, but with permutated projected vertices. (*b*) By shifting the acceptance window along perp-space, different tilings can be produced in the canonical description. Three tilings as created from 7D space by placing the center of the window at $(000000k)_V$, with (left) $k = 0$ (singular case), (center) $k = 0.75$, (right) $k = 1.25$, with $a^* = 2/7^{1/2}$. (*c*) Unit cell of the PAS with overlapping PHSs. Depicted are all symmetrically non-equivalent PASs that correspond to the diffraction vectors $(10\bar{1}1011)_{\mathbf{D}^*}$ and $(10\bar{1}\bar{1}101)_{\mathbf{D}^*}$ (left), $(110\bar{1}101)_{\mathbf{D}^*}$ (center) and $(110\bar{1}\bar{1}10)_{\mathbf{D}^*}$ (right). In all cases the PHSs almost fill the unit cell of the PAL. Black lines mark the outer boundary of the PHSs, points result from the 7-QPT modulo one unit cell of the PAL. a_{PAS} (in units of a_r) and p_{PAS} are given in the figure. (*d*) Decomposition of the PHS in the individual parts for one PAS. (*e*) PASs corresponding to the diffraction vectors $(1\bar{1}\bar{2}2022)_{\mathbf{D}^*}$ and $(20\bar{2}\bar{2}1\bar{1}2)_{\mathbf{D}^*}$ (left), $(21\bar{1}\bar{2}202)_{\mathbf{D}^*}$ (center), $(220\bar{2}\bar{2}\bar{1}1)_{\mathbf{D}^*}$ (right).

unusual properties, as do tilings with axial symmetries 9, 11 and greater than 12. Since all tilings with those symmetries considered within this work are canonical projection tilings, they all fulfill the Pisot–Vijayaraghavan property (Vijayaraghavan, 1941) as required for finite (non-fractal) HSs and have a pure point Fourier spectrum. Consequently, those tilings cannot be substitution tilings (Harriss, 2005).

5.2. PASs

Since the QPTs are described with a reducible nD basis, $(n-2)$D projections are necessary to generate the corresponding PASs. Thereby, the dimension $(n-3)$ of the HSs is reduced to 2. This has direct implications on the distribution functions of the deviations of the QPT vertices from the respective PALs. In the eight- and tenfold cases this distribution can be described as a simple step function. For all tilings with HSs of a dimension higher than two, however, the distribution of deviations corresponds to the onto par-space projected volume function of the HSs. Consequently, the higher the dimensionality of the HSs the more complex this function becomes.

In the following, several symmetrically non-equivalent PASs, with p_{PAS} close to 1, will be discussed for the 7-QPT. For this purpose, two reflections with strong intensities are chosen, that are related to PAS lattice parameters close to the tiling edge length. The resulting PAS unit cells correspond to the three different unit tiles of the 7-QPT. In these PASs [Figs. 5(*c*) and 5(*d*)], the symmetry of the HSs is not preserved in the oblique projections, and PHSs that are centered around neighboring PAS nodes can show large overlaps (Fig. 5*c*). The decomposition of heavily overlapping PHSs [Fig. 5(*c*), right side] is shown in Fig. 5(*d*).

The best PAS for the 7-QPT [Fig. 5(*c*), left side] has a p_{PAS} close to 1 (only 4% of the PAS unit tiles are not occupied), but its unit cell is almost completely covered with PHSs. On the other hand, the best PAS with small maximal deviation of the tiling vertices from the lattice nodes [Fig. 5(*e*), left side] has only a p_{PAS} of 0.5670. Almost half of the PHSs are not occupied. The 7-QPT shows therefore a low DAP; it resembles a strongly density (vacancy) modulated structure.

Even lower DAPs are calculated for the 11-QPT and the 13-QPT. From a general point of view, for every QPT PASs can be constructed with very small deviations of the tiling vertices from the PAL nodes. For the limit of the PAS unit-cell parameters approaching zero, the deviations of the tiling vertices also go to zero, as well as the p_{PAS} of the PHSs however. In this case, the description of a QPT by its PAS no longer makes any sense from a physical point of view.

In Figs. 6 and 7, an 11-QPT and a 13-QPT, respectively, are shown together with their PASs. Furthermore, the growth of the PHSs as a function of the patch size of finite tilings modulo one unit cell is illustrated in several examples. In the case of

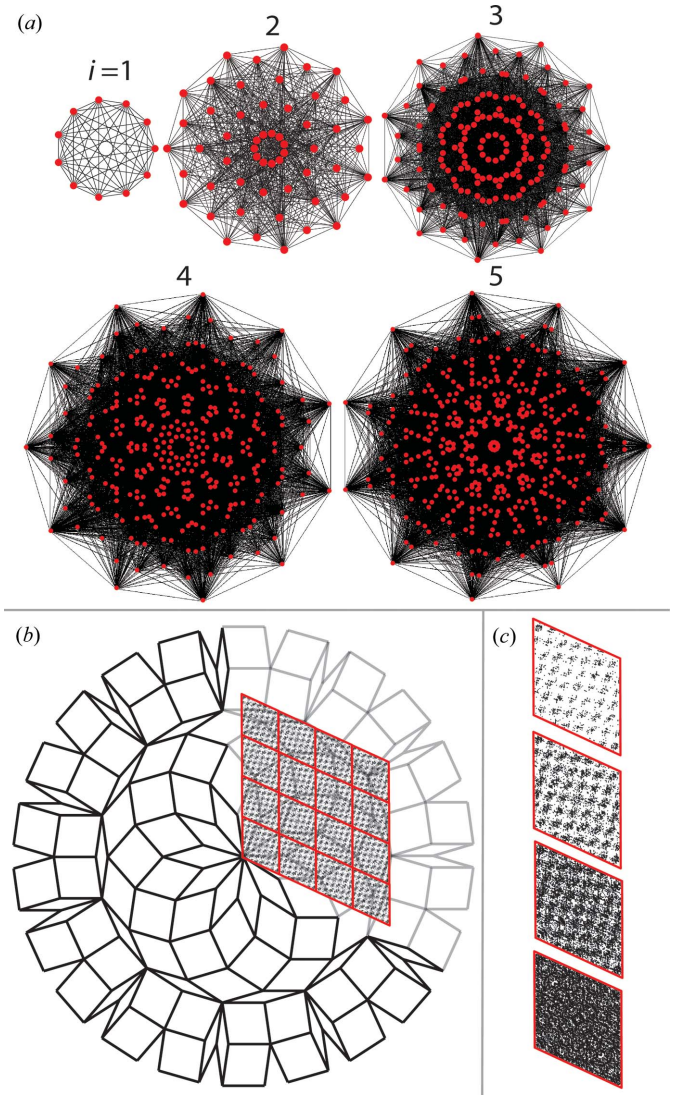

Figure 6
(*a*) The 11 HSs of the 11-QPT are located on $(i/11)(11111111111)_{\mathbf{D}}$, i = 0, . . . , 10, in the canonical description. They are related by an inversion center in the origin and at $1/2(11111111111)_{\mathbf{D}}$. The HSs are 8D polytopes. They are shown in an orthogonal projection upon one of the four 2D invariant subspaces of $\mathbf{V}^{\perp}$. (*b*) Tiling with overlaid PAS. (*c*) PAS and a finite tiling modulo one unit cell of the PAL, for four different patch sizes of the 11-QPT, growing from top to bottom (radii of the tilings/number of vertices: 20/1585, 35/4841, 50/9923 and 65/16831). The diffraction vectors defining the PAS are $(1101\bar{1}\bar{1}\bar{1}\bar{1}\bar{1}\bar{1}01)_{\mathbf{D}^*}$ and the symmetrically equivalent one that gives basis vectors of the PAL with the opening angle $4\pi/11$.

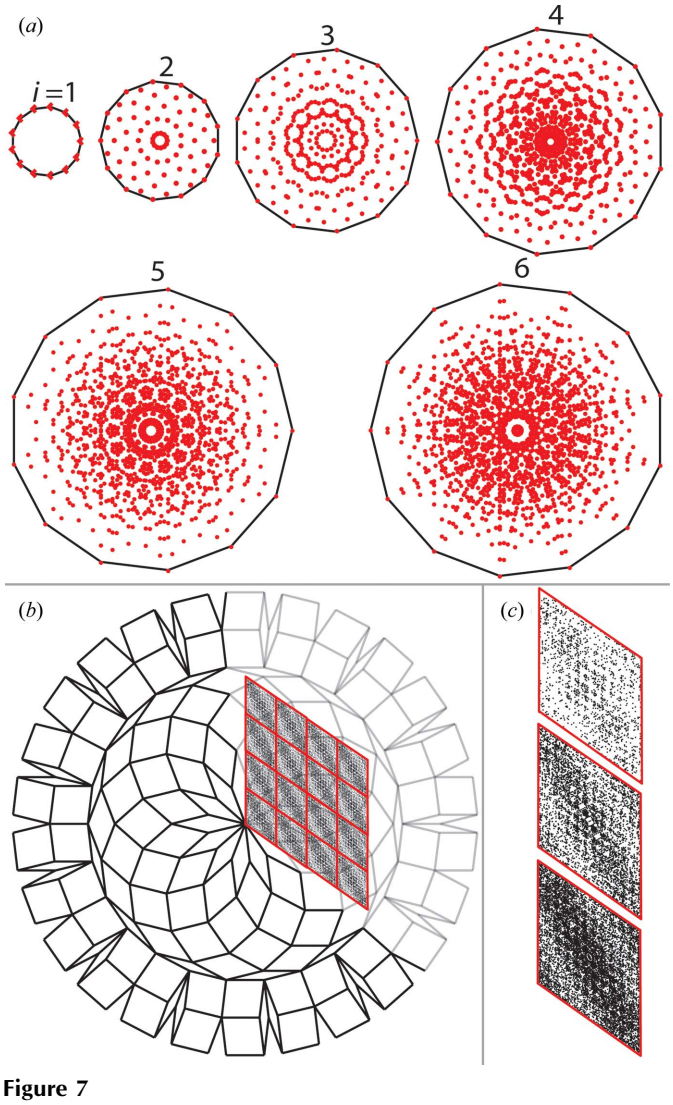

Figure 7
(*a*) The 13 HSs of the 13-QPT are located on $(i/13)(1111111111111)_{\mathbf{D}}$, i = 0, . . . , 12, in the canonical description. They are related by an inversion center in the origin and at $1/2(1111111111111)_{\mathbf{D}}$. The HSs are 10D polytopes. They are shown in an orthogonal projection upon one of the four 2D invariant subspaces of $\mathbf{V}^{\perp}$. (*b*) Tiling with overlaid PAS. (*c*) PAS and a finite tiling modulo one unit cell, for three different patch sizes of the 13-QPT, growing from top to bottom (radii of the tilings/number of vertices: 20/1574, 35/4876 and 50/9894). The diffraction vectors defining the PAS are $(1110\bar{1}\bar{1}\bar{1}\bar{1}\bar{1}\bar{1}\bar{1}011)_{\mathbf{D}^*}$ and the symmetrically equivalent one that gives basis vectors of the PAL with the opening angle $4\pi/13$.

infinite QPTs taken modulo one unit cell of their respective PASs, the vertices would fill the unit cells densely.

In the case of the 11-QPT, the reciprocal PAS unit cell is defined by the reflection $1101\bar{1}\bar{1}\bar{1}\bar{1}\bar{1}\bar{1}01$ and its symmetrically equivalent counterpart that gives a PAL with an angle $4\pi/11$ between the basis vectors in direct par-space. The unit-cell parameters result in $a_{\rm PAS} = 0.9759a_r$. The radii of the finite QPT patches are (from top to bottom of Fig. 7*c*) 20, 35, 50 and 65, with the number of vertices 1585, 4841, 9923 and 16831, respectively.

In the case of the 13-QPT, the reciprocal PAS unit cell is spanned by the reflection $1110\bar{1}\bar{1}\bar{1}\bar{1}\bar{1}\bar{1}\bar{1}011$ and its symmetrically equivalent counterpart that gives a PAL with an angle $4\pi/13$ between the basis vectors in direct par-space. The unit-cell parameters result in $a_{\rm PAS} = 0.9805a_r$. The radii of the finite QPT patches are (from top to bottom of Fig. 7*c*) 20, 35 and 50, with the number of vertices 1574, 4876 and 9894, respectively.

6. Dodecagonal, enneagonal and pentakaidecagonal tilings (12-, 9- and 15-QPTs)

6.1. Formalism

All diffraction vectors $\mathbf{H}^{\parallel}$ of N-QPTs with N = 12, 9 and 15 can be represented on a 2D par-space basis with vectors $\mathbf{a}_i^*$ =

$a^*[\cos(2\pi i/N), \sin(2\pi i/N)]$, with $i = 1, \ldots, N$. The projected nD diffraction vectors are given by $\mathbf{H}^{\parallel} = \sum_{i=1}^{N} h_i \mathbf{a}_i^*$. Based on the number of independent reciprocal basis vectors necessary to index the diffraction vectors with integers, the rank of the Z-module and the dimension of the embedding spaces in their irreducible variants results to 4, 6 or 8, respectively. In the canonical description, 6, 9 or 15D, respectively, hyperlattices are needed to generate the QPTs.

For the 12-QPT, the nD hypercubic lattice (**D** basis) is given by the vectors

$$\mathbf{d}_i = \frac{1}{3a^*} \begin{pmatrix} 1 & c_1 & -c_2 & -c_3 & c_4 & c_2 \\ 0 & s_1 & -s_2 & -s_3 & s_4 & s_2 \\ 1 & c_5 & c_4 & -c_3 & -c_2 & c_1 \\ 0 & s_5 & s_4 & -s_3 & -s_2 & s_1 \\ \frac{1}{\sqrt{2}} & -\frac{1}{\sqrt{2}} & \frac{1}{\sqrt{2}} & -\frac{1}{\sqrt{2}} & \frac{1}{\sqrt{2}} & -\frac{1}{\sqrt{2}} \\ \frac{1}{\sqrt{2}} & \frac{1}{\sqrt{2}} & \frac{1}{\sqrt{2}} & \frac{1}{\sqrt{2}} & \frac{1}{\sqrt{2}} & \frac{1}{\sqrt{2}} \end{pmatrix}_{\mathbf{v}}, \qquad (8)$$

with $i = 1, \ldots, 6$. The unit tiles edge length a_r is related to the length a^* of the 2D par-space reciprocal basis vectors by $a_r = 1/3a^*$. The 12-QPT has, in the canonical description, three orthogonal subspaces spanned by the vectors $\mathbf{v}_0$ and $\mathbf{w}_0$ (par-space $\mathbf{V}^{\parallel}$), and $\mathbf{v}_k$ and $\mathbf{w}_k$ (perp-space $\mathbf{V}_k^{\perp}$ for $k = 1, 2$). $\mathbf{V}$ is then decomposed to $\mathbf{V} = \mathbf{V}^{\parallel} \oplus \mathbf{V}^{\perp} = \mathbf{V}^{\parallel} \oplus \mathbf{V}_1^{\perp} \oplus \mathbf{V}_2^{\perp}$. In the **D** basis, they can be expressed as $\mathbf{v}_k = (1/3^{1/2}a^*) \times \cos[(k+1)2\pi i/12]_{\mathbf{D}}$, $\mathbf{w}_k = (1/3^{1/2}a^*)\sin[(k+1)2\pi i/12]_{\mathbf{D}}$. The vector $\mathbf{w}_2$ corresponds to the usual diagonal $\mathbf{d} = (1/3^{1/2}a^*)(1/2^{1/2})(111111)_{\mathbf{D}}$ of the nD unit cell, while $\mathbf{v}_2 = (1/3^{1/2}a^*)(1/2^{1/2})(1\bar{1}1\bar{1}1\bar{1})_{\mathbf{D}}$ is a diagonal vector in a different direction. Both these directions are redundant, and together they build a 2D subspace ($\mathbf{V}_2^{\perp}$) to which the HSs are orthogonal. This is illustrated in Fig. 8. The HSs are 2D and given by six equidistant cuts of the window perpendicular to the redundant directions at $(i/6)(\mathbf{v}_2 + \mathbf{w}_2) = (i/6)(1\bar{1}1\bar{1}1\bar{1})_{\mathbf{D}} + (111111)_{\mathbf{D}}$ with $i = 1, \ldots, 6$. The 12-QPT is generated by a window which is centered at the origin of the hyperlattice.

The ninefold tiling has five orthogonal subspaces. Therein, the vectors $\mathbf{v}_0$ and $\mathbf{w}_0$ span the 2D par-space $\mathbf{V}^{\parallel}$, $\mathbf{v}_k$ and $\mathbf{w}_k$ span $\mathbf{V}_k^{\perp}$ for $k = 1, \ldots, 3$, and $\mathbf{d}$ spans $\mathbf{V}_4^{\perp}$, with $\mathbf{V} = \mathbf{V}^{\parallel} \oplus \mathbf{V}^{\perp} = \mathbf{V}^{\parallel} \oplus \mathbf{V}_1^{\perp} \oplus \mathbf{V}_2^{\perp} \oplus \mathbf{V}_3^{\perp} \oplus \mathbf{V}_4^{\perp}$. It is $\mathbf{v}_k = (2/9)^{1/2}(1/a^*) \times \cos[(k+1)2\pi i/9]_{\mathbf{D}}$, $\mathbf{w}_k = (2/9)^{1/2}(1/a^*)\sin[(k+1)2\pi i/9]_{\mathbf{D}}$ and $\mathbf{d} = (1/9^{1/2}a^*)(111111111)_{\mathbf{D}}$.

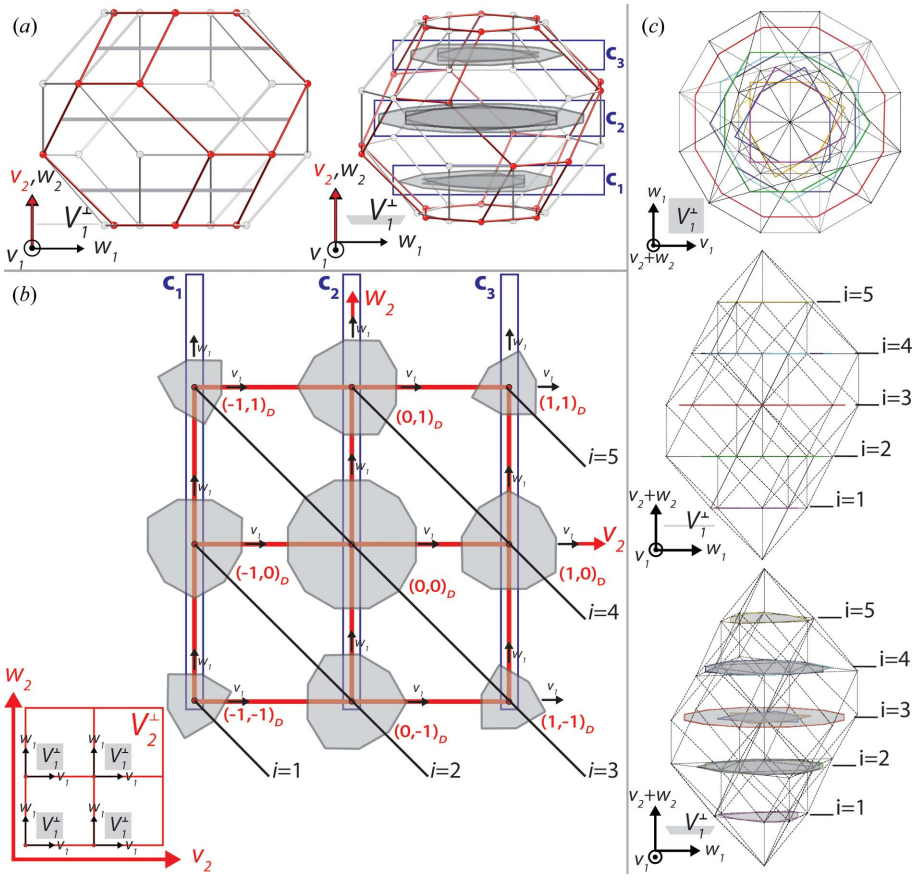

Figure 8
(*a*) Window function of the 12-QPT shown simultaneously for dimensions $\mathbf{V}_1^{\perp} \oplus \mathbf{v}_2$ and $\mathbf{V}_1^{\perp} \oplus \mathbf{w}_2$, with the HSs in the projection upon $\mathbf{V}_1^{\perp} \oplus \mathbf{w}_2$. They belong to three groups, denoted $\mathbf{c}_1$, $\mathbf{c}_2$, $\mathbf{c}_3$, each consisting of three HSs. (*b*) MCS plot of the HSs resulting from cuts of the strip centered at the origin of the hyperlattice. The gray outlines of each HS are given in a subplot of $\mathbf{V}_1^{\perp}$, on each node of $\mathbf{V}_2^{\perp}$. The positions of the HSs in $\mathbf{V}_2^{\perp}$ are plotted by their occupation of nodes on the red grid spanned by $\mathbf{v}_2$ and $\mathbf{w}_2$. (*c*) The HSs are given by six equidistant cuts of the window perpendicular to $\mathbf{V}_2^{\perp}$, along the direction $\mathbf{v}_2 + \mathbf{w}_2$.

The strip cuts a 7D slab parallel to the 2D par-space from the 9D lattice. The HSs are given by nine equidistant cuts perpendicular to **d**. For every additional redundant dimension ($\mathbf{v}_2$ and $\mathbf{w}_2$), the HSs are subdivided into sets of HSs, as shown in Fig. 9. This means that none of the HSs has a volume in $\mathbf{V}_2^{\perp}$, but separate HSs cut $\mathbf{V}_2^{\perp}$ at different coordinates. The resulting HSs are of the dimension 0, 2 and 4. Fig. 9(*b*) shows a MCS plot of the four sets of independent HSs, in $\mathbf{V}_2^{\perp}$ and $\mathbf{V}_1^{\perp}$. They are located at $i/9(111111111)_{\mathbf{D}}$, $i = 1, \ldots, 4$, related to the HSs at $i/9(111111111)_{\mathbf{D}}$, $i = 5, \ldots, 8$, by an inversion center in the origin and at $1/2(111111111)_{\mathbf{D}}$. Projection upon $\mathbf{V}_3^{\perp}$ would give the same image as projection upon $\mathbf{V}_2^{\perp}$, but with permutated vertices.

The nD hypercubic lattice (**D** basis) is given by the vectors

$$\mathbf{d}_i = \frac{2}{9a^*} \begin{pmatrix} \cos(2\pi i/9) \\ \sin(2\pi i/9) \\ \cos(4\pi i/9) \\ \sin(4\pi i/9) \\ \cos(6\pi i/9) \\ \sin(6\pi i/9) \\ \cos(8\pi i/9) \\ \sin(8\pi i/9) \\ 1/\sqrt{2} \end{pmatrix}_{\mathbf{v}}, \qquad (9)$$

with $i = 1, \ldots, 9$. The unit tiles edge length a_r is related to the length a^* of the 2D par-space reciprocal basis vectors by $a_r = 2/9a^*$.

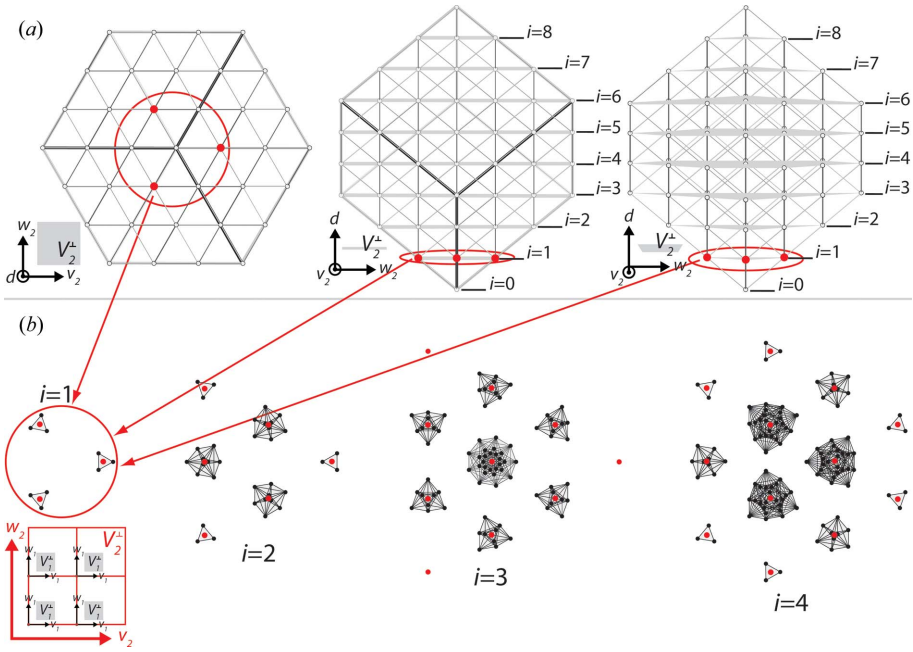

Figure 9
(*a*) Three views of the window of the 9-QPT in the canonical 9D description. The HSs are perpendicular to $\mathbf{V}_2^{\perp}$ and **d**. Each node shown in (*a*) represents therefore one HS located on nine equidistant cuts perpendicular to **d**, as indicated in gray on the right. (*b*) MCS plot of the four sets of independent HSs, located at $i/9(111111111)_{\mathbf{D}}$, $i = 1, \ldots, 4$. They are related to the HSs at $i/9(111111111)_{\mathbf{D}}$, $i = 5, \ldots, 8$, by an inversion center in the origin and at $1/2(111111111)_{\mathbf{D}}$. The non-trivial HSs are 2D and 4D polytopes, and have only a volume in $\mathbf{V}_1^{\perp}$ and $\mathbf{V}_3^{\perp}$. Their positions in $\mathbf{V}_2^{\perp}$ are given by red dots, and their projected volume in $\mathbf{V}_1^{\perp}$ is given in black. The lines give the convex hull of the HSs. The dimensionality of the non-trivial HSs is 2 and 4. Projection upon $\mathbf{V}_3^{\perp}$ would give the same image as projection upon $\mathbf{V}_2^{\perp}$, but with permutated vertices.

The 15-fold tiling is analogous to the ninefold tiling, with three additional perp-subspaces, where the last one, $\mathbf{V}_7^{\perp}$, is spanned by **d**. It is $\mathbf{v}_k = (2/15)^{1/2}(1/a^*)\cos[(k+1)2\pi i/15]_{\mathbf{D}}$, $\mathbf{w}_k = (2/15)^{1/2}(1/a^*)\sin[(k+1)2\pi i/15]_{\mathbf{D}}$ and $\mathbf{d} = (1/15^{1/2}a^*) \times (111111111111111)_{\mathbf{D}}$. The unit tiles edge length a_r is related to the length a^* of the 2D par-space reciprocal basis vectors by $a_r = 2/15a^*$, and the nD hypercubic lattice (**D** basis) is given by the vectors

$$\mathbf{d}_i = \frac{2}{15a^*}\begin{pmatrix} \cos(2\pi i/15) \\ \sin(2\pi i/15) \\ \cos(4\pi i/15) \\ \sin(4\pi i/15) \\ \cos(6\pi i/15) \\ \sin(6\pi i/15) \\ \cos(8\pi i/15) \\ \sin(8\pi i/15) \\ \cos(10\pi i/15) \\ \sin(10\pi i/15) \\ \cos(11\pi i/15) \\ \sin(11\pi i/15) \\ \cos(12\pi i/15) \\ \sin(12\pi i/15) \\ 1/\sqrt{2} \end{pmatrix}_{\mathbf{V}}, \quad \text{with } i = 1, \ldots, 15. \qquad (10)$$

The strip cuts a 13D slab parallel to the 2D par-space from the 15D lattice. There are 15 HS sets in the canonical description, located at $i/15(111111111111111)_{\mathbf{D}}$, $i = 0, \ldots, 14$, and related by an inversion center in the origin and at $1/2(111111111111111)_{\mathbf{D}}$. They have a volume only in the subspaces $\mathbf{V}_1^{\perp}$, $\mathbf{V}_3^{\perp}$ and $\mathbf{V}_6^{\perp}$, and are perpendicular to all others. Fig. 10 shows the HS sets at $i = 4, \ldots, 7$ in a detailed MCS plot.

6.2. PASs

The best PAS for the 12-QPT is shown in Fig. 11(*b*) (top). The corresponding reflections are $01\bar{2}\bar{1}00$ and $21000\bar{1}$. The unit-cell parameter of the centered PAS is $a_{\mathrm{PAS}} = 0.9282$, and only 7% of the unit tiles of the PAS do not contain a tiling vertex. The distribution of vertices is uniform in each PHS, and the deviation density adds up with the number of overlapping PHSs within their boundaries. A PAS without centering and with small maximal deviation of the vertices from the PAL nodes is given in Fig. 11(*b*) (bottom). Here, all HSs project onto each other. The corresponding reflections are $01\bar{2}\bar{1}00$ and $21000\bar{1}$, the unit-cell parameter of the PAS is $a_{\mathrm{PAS}} = 0.4641$, and $p_{\mathrm{PAS}} = 0.2679$ is very small. The symmetry of the HSs is preserved by the oblique projections in both PASs.

An example of a 9-QPT is shown in Fig. 12(*a*). It is generated from a 9D hypercubic lattice by placing the center of the window at $(00000000k)_{\mathbf{V}}$, with $k = 0.001$. The best PAS for the 9-QPT is shown in Fig. 12(*b*). The reflection $1110\bar{2}\bar{2}\bar{2}\bar{2}0$ and one of its symmetrically equivalent counterparts are chosen to obtain a PAL with an angle $6\pi/9 = 2\pi/3$ between the basis vectors. The unit-cell parameter of the PAS is $a_{\mathrm{PAS}} = 0.6267$. The PAS has $p_{\mathrm{PAS}} = 1.2344$ and a rather small maximal deviation of the tiling vertices from the PAL nodes. The PHSs are centered at three sites: $(0\,0)_{\mathbf{PAS}}$, $(1/3\,2/3)_{\mathbf{PAS}}$ and $(2/3\,1/3)_{\mathbf{PAS}}$. The density distribution of deviations from the PAL corresponds to the volume function of the PHS. As in the case of the 7-QPT, the 4D HSs project onto the 2D par-space and give a non-homogeneous point distribution in the PAS. Contrary to the case of the 7-QPT, however, there is a PAS with small maximal deviation and reasonable p_{PAS}.

In the case of the 15-QPT, the DAP does not allow a representative description of the infinite QPT *via* one of its PASs, analogously to the cases of the 11- and 13-QPT. In Fig. 13(*a*) a 15-QPT is depicted, and in (*b*)–(*d*) a PAS and a finite patch of the 15-QPT modulo one unit cell are shown for three different patch sizes. The infinite tiling taken modulo one unit cell of the PAS would fill the cell densely and inhomogeneously. The corresponding reflections chosen for the PAS in (*b*) are $0100\bar{1}\bar{1}\bar{1}\bar{1}\bar{1}\bar{1}\bar{1}\bar{1}\bar{1}\bar{1}\bar{1}\bar{1}11$, and in (*c*) and (*d*) $1111001\bar{1}\bar{1}\bar{1}\bar{1}\bar{1}\bar{1}011$. The opening angles of the PAL basis vectors are $4\pi/15$ in (*b*) and (*c*), and $10\pi/15 = 2\pi/3$ in (*d*).

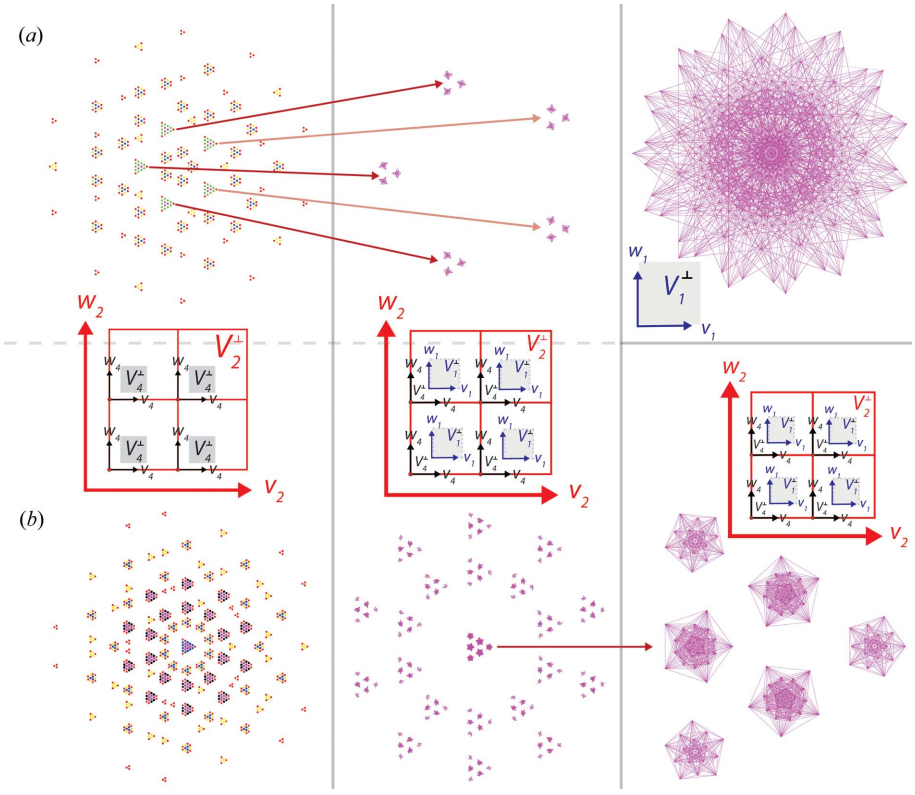

Figure 10
In the case of the 15-QPT, there are 15 HS sets in the canonical description, located at $i/15(111111111111111)_{\mathbf{D}}$, $i = 0, \ldots, 14$. They are related by an inversion center in the origin and at $1/2(111111111111111)_{\mathbf{D}}$. They have a volume only in the subspaces $\mathbf{V}_1^\perp$, $\mathbf{V}_3^\perp$ and $\mathbf{V}_6^\perp$, and are perpendicular to all others. The HS sets, resulting from the cuts at $i = 4$ and 5, are shown in a MCS plot. The HSs are perpendicular to $\mathbf{V}_2^\perp$ and $\mathbf{V}_4^\perp$. Their positions in these two subspaces are marked on the left. Different colors indicate different dimensionalities of the HSs. Dimension/color: 6/purple, 5/blue, 4/green, 3/black, 2/cyan and 0,1/red. Only the six-dimensional HSs are shown in the middle part of (*a*) and (*b*), in a MCS plot with one additional subspace. On the right side of (*a*) the six-dimensional HSs for $i = 4$ are shown in an orthogonal projection on $\mathbf{V}_1^\perp$, as opposed to the combined scaling plot of $\mathbf{V}_2^\perp$, $\mathbf{V}_4^\perp$ and $\mathbf{V}_1^\perp$ in the middle. On the right side of (*b*) the central nine HSs at $i = 5$ are shown enlarged, again in a combined scaling plot. The lines give the convex hulls of the HSs.

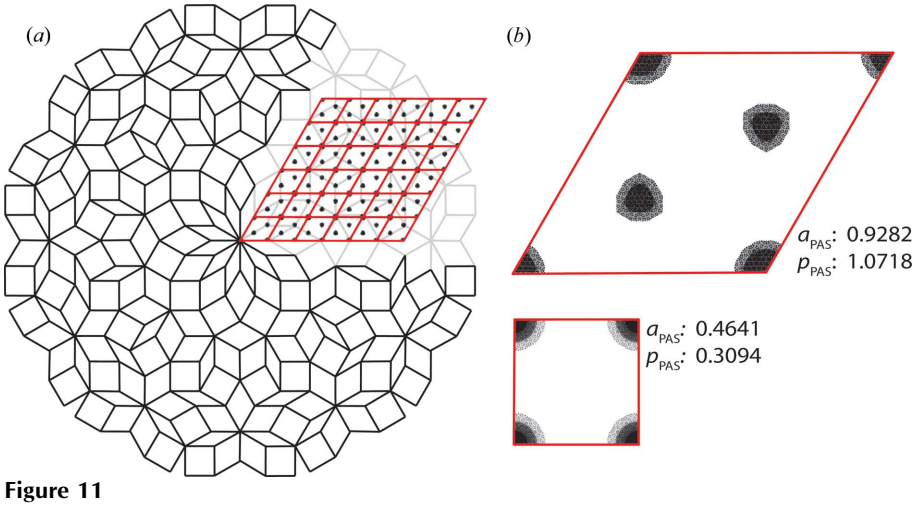

Figure 11
(*a*) 12-QPT generated by the canonical projection method, with the acceptance window centered at the origin of the 6D lattice. (*b*) (Top) Centered PAS with overlapping PHSs. The chosen diffraction vectors are $(01\bar{2}\bar{1}00)_{\mathbf{D}^*}$ and $(210001)_{\mathbf{D}^*}$. (Bottom) PAS with complete overlap of the HSs belonging to one lattice node and small maximal deviation of the tiling vertices from the PAL. The reciprocal lattice of the PAS is defined by the diffraction vectors $(320002\bar{)}_{\mathbf{D}^*}$ and $(00\bar{2}\bar{3}20)_{\mathbf{D}^*}$. a_{PAS} (in units of a_r) and p_{PAS} are given in the figure.

7. Concluding remarks

The PASs of the 2D QPTs with diffraction symmetries N = 7, 8, 9, 10, 11, 12, 13 and 15 strongly differ in the size of the PHSs relative to the unit-cell dimensions and in their p_{PAS}. Since the vertex distribution in an nD HS is homogeneous, so is the projection of one single HS, if its dimension is not reduced by the projection. This is, for instance, the case for the eight- and tenfold tilings.

In the case of 7-, 9-, 11-, 12-, 13- and 15-QPTs, the vertices originate from several HSs, which overlap in their projection for all PASs of physical relevance (*i.e.* those generated by reflections with strong intensities). In the case of the 12-QPT, the HSs and their projections are 2D and homogeneous. However, parts of the HSs are projected upon each other in the PAS. The resulting density distribution can then be described by a simple step function, following the boundaries of the single PHSs and their overlaps. There is a noticeable similarity between the PASs of the 9-QPT and the 12-QPT, which both have a simple factorization into parameters related to crystallographic symmetries: $9 = 3 \times 3$ and $12 = 3 \times 4$.

The cases of the 7-, 9-, 11-, 13- and 15-QPTs, however, are more complicated than that of the 12-QPT, since they all have more HSs whose dimensionality is reduced by their projection onto 2D par-space. The projected density distribution is therefore not homogeneous.

Although the density distribution of a PAS can be taken as a measure of the DAP of the respective QPT, this concept has to be treated carefully. It is only reliable if the total diffraction intensity represented by the PAS is large, and if p_{PAS} of the PHS is close to 1. The 8-, 10- and 12-QPTs, for instance, can be closely represented by their PAS. The 7- and 9-QPTs show a higher degree of complexity in their PAS, and, finally, the 11-, 13- and 15-QPTs elude a reasonable periodic approximation and show the lowest DAP and, consequently, the highest degree of quasiperiodicity.

There is a clear general trend to a lower DAP with increasing rank of the

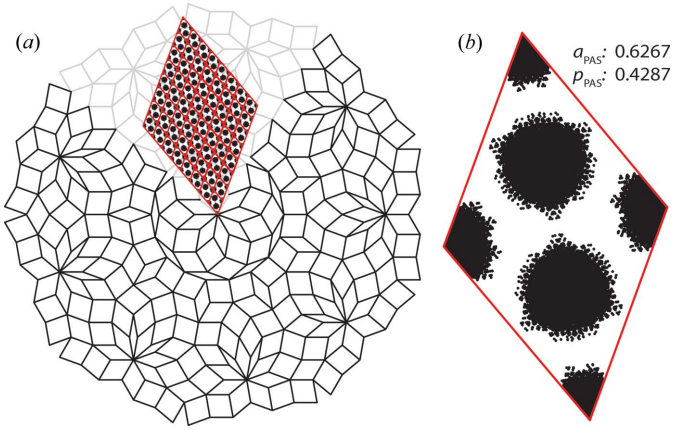

Figure 12
(*a*) 9-QPT with overlaid PAS, generated from a 9D hypercubic lattice by placing the center of the window at $(00000000k)_{\mathbf{V}}$, with $k = 0.001$. (*b*) Unit cell of the PAS defined by the diffraction vectors $(1110\bar{2}\bar{2}\bar{2}0)_{\mathbf{D}^*}$ and $(\bar{2}\bar{2}01110\bar{2}\bar{2})_{\mathbf{D}^*}$ (opening angle $6\pi/9 = 2\pi/3$). $a_{\rm PAS}$ (in units of a_r) and $p_{\rm PAS}$ are given in the figure.

QPT (minimum dimensionality of the embedding space **V**). This is true for both N prime or non-prime within their own categories. N-QPTs with N non-prime and of low dimensionality show the best, most distinct, PASs and have the highest DAP.

This is in agreement with observations of occurring symmetries and stability of metallic as well as soft quasicrystals, and gives us a geometrical interpretation of the observed trends. Generally speaking, the higher the dimensionality of a system, the lower is the DAP, and it is also less physically favorable; N being a non-prime number seems to be advantageous over N being a prime number.

Many thanks go to Daniel Sutter-Widmer for fruitful discussions and support. Financial support under grant SNF 200020-121568 is gratefully acknowledged.

References

Ammann, R., Grünbaum, B. & Shephard, G. C. (1992). *Discrete Comput. Geom.* **8**, 1–25.
Baake, M. & Grimm, U. (2011). *Z. Kristallogr.* **226**, 711–725.

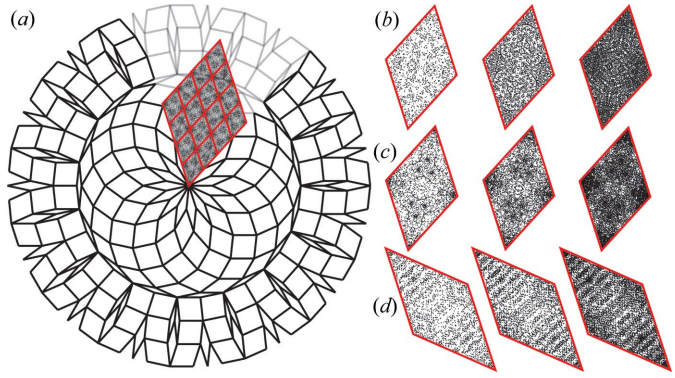

Figure 13
(*a*) 15-QPT with overlaid PAS, generated from a 15D hypercubic lattice by placing the center of the window at $(000000000000000k)_{\mathbf{V}}$, with $k = 0.001$. (*b*)–(*d*) PAS and finite patch of the 15-QPT modulo one unit cell for three different patch sizes, increasing from left to right (radii of the tilings/number of vertices: 20/1591, 35/4801 and 50/9991). The diffraction vectors defining the PAS in (*b*) are $(0100\bar{1}\bar{1}\bar{1}\bar{1}\bar{1}\bar{1}\bar{1}\bar{1}111)_{\mathbf{D}^*}$, in (*c*) and (*d*) $(111100\bar{1}\bar{1}\bar{1}\bar{1}\bar{1}\bar{1}011)_{\mathbf{D}^*}$. The opening angles are in (*b*) and (*c*) $4\pi/15$, in (*d*) $10\pi/15 = 2\pi/3$.

Bruijn, N. G. de (1981). *Proc. Kon. Ned. Akad. Wet. Ser. A*, **84**, 39–52.
Cervellino, A. & Steurer, W. (2002). *Acta Cryst.* A**58**, 180–184.
Fischer, S., Exner, A., Zielske, K., Perlich, J., Deloudi, S., Steurer, W., Lindner, P. & Förster, S. (2011). *Proc. Natl Acad. Sci. USA*, **108**, 1810–1814.
Harriss, E. O. (2005). *Discrete Comput. Geom.* **34**, 523–536.
Masakova, Z., Patera, J. & Zich, J. (2005). *J. Phys. A*, **38**, 1947–1960.
Moody, R. V. & Patera, J. (2000). *Model Sets: A Survey*. In *From Quasicrystals to More Complex Systems.* Berlin: Springer Verlag.
Socolar, J. E. S. (1989). *Phys. Rev. B*, **39**, 10519–10551.
Steurer, W. (2000). *Z. Kristallogr.* **215**, 323–334.
Steurer, W. & Deloudi, S. (2008). *Acta Cryst.* A**64**, 1–11.
Steurer, W. & Deloudi, S. (2009). *Crystallography of Quasicrystals: Concepts, Methods and Structures*. *Series in Materials Science*, Vol. 126. Berlin: Springer.
Steurer, W. & Haibach, T. (1999). *Acta Cryst.* A**55**, 48–57.
Steurer, W. & Sutter-Widmer, D. (2007). *J. Phys. D*, **40**, R229–R247.
Sutter-Widmer, D., Deloudi, S. & Steurer, W. (2007*a*). *Philos. Mag.* **87**, 3095–3102.
Sutter-Widmer, D., Deloudi, S. & Steurer, W. (2007*b*). *Phys. Rev. B*, **75**, 094304.
Vijayaraghavan, T. (1941). *Proc. Cambridge Philos. Soc.* **37**, 349–357.
Weisskopf, Y., Burkardt, S., Erbudak, M. & Longchamp, J. N. (2007). *Surf. Sci.* **601**, 544–551.